

The Numerical Assembly Technique for arbitrary planar systems based on an alternative homogeneous solution

Thomas Kramer^{a,*}, Michael Helmut Gfrerer^a

^a*Institute of Applied Mechanics
University of Technology Graz
Technikerstraße 4, 8010 Graz, Austria*

Abstract

The Numerical Assembly Technique is extended to investigate arbitrary planar frame structures with the focus on the computation of natural frequencies. This allows us to obtain highly accurate results without resorting to spatial discretization. To this end, we systematically introduce a frame structure as a set of nodes, beams, bearings, springs, and external loads and formulate the corresponding boundary and interface conditions. As the underlying homogeneous solution of the governing equations, we use a novel approach recently presented in the literature. This greatly improves the numerical stability and allows the stable computation of very high natural frequencies accurately. We show this numerically at two frame structures by investigation of the condition number of the system matrix and also by the use of variable precision arithmetic.

Keywords: Dynamic analysis of frames, Numerical Assembly Technique, NAT, Euler-Bernoulli beam theory, Natural frequencies, Mode shapes, Analytical solution, Variable precision arithmetic

*kramer@tugraz.at

1. Introduction

A significantly high number of mechanical and structural engineering problems can be modeled by an assembly of beams with attached supports, hinges, and springs such as building structures but also robotic arms or any mechanical mechanism. Especially for structural features where the dynamic behavior is of major interest, the natural frequencies play an important role. Thus, having an efficient tool to determine those natural frequencies, combined with the corresponding mode shapes, helps engineers perform high-quality work.

For simple problems analytical formulas can be found in various textbooks [1]-[4]. There, functions to compute natural frequencies and mode shapes are derived for e.g. cantilever beams or single-span beams with various supports. Also for more complicated systems a huge amount of analytical and semi-analytical methods can be found in the literature. A detailed literature review can be found in [5].

One widely used method is the Dynamic Stiffness Method (DSM) which uses shape functions tailored to the governing equations and the assembly technique from the Finite Element Method [6]. Due to its general structure, it can be applied to arbitrary frame structures. Recently, it has been extended to functionally graded beams [7] and axially loaded multi-cracked frames [8] among other extensions such as beams carrying spring-mass systems [9] and axially loaded composite Timoshenko beams [10].

To analyze multi-stepped beams with various concentrated masses the Transfer Matrix Method (TMM) is often used. With this approach, a matrix transfers the beam state such as the displacement, the rotation, the internal forces, and the bending moment from one end of a uniform beam segment to the other. Anyway, this method's application is limited to multi-span [11] or multi-stepped beams [12] and can, therefore, not be applied on plane frame structures. Also, this method has been extended to crack identification of stepped beams with multiple edge cracks and different boundary conditions [13].

Another noteworthy method is the Green Function Method (GFM), which

uses the analytical responses of a uniform beam segment to point loads (Green functions) to include concentrated elements in the beam model. It is left to solve for the displacement and the rotations of the beam at each element. Hence, the size of the system matrix depends clearly on the number of concentrated elements. Lately, this method has been used to analyze elastically supported Euler-Bernoulli beams [14], cracked beams with elastic boundary conditions [15] and axially functionally graded and non-uniformed beams [16].

The Generalized Function Approach (GFA) follows a similar idea as the GFM, where the discontinuous response of the beam due to concentrated elements and the changes in material parameters is handled with generalized functions such as Dirac delta functions or Heaviside step functions. Contrarily to the GFM, the size of the system matrix is independent of the number of uniform beam sections. A plane vibration problem can, therefore, be assembled by a 2×2 system matrix. The GFA has been extensively studied. Most recently on beams with various in-span supports and masses [17], on discontinuous layered elastically bonded beams [18], on plane structures with mass-spring subsystems and rotational joints [19] and on beams including tuned mass dampers with spring inertia effects [20].

The Numerical Assembly Technique (NAT) considers the analytical solution of the homogeneous governing equation. Each analytical solution with the enforced boundary and intermediate conditions holds within a uniform beam segment and occupies one row in the system of equations. Hence, the implementation is straight forward and the size of the system of equations rises with the complexity of the structure.

Numerous research papers concerning the NAT have been published. Whereas two authors have caught our attention specifically throughout the literature studies as they are certainly experts in this field of research. Their most recent publications regarding the NAT are the computation of steady-state harmonic vibrations of viscoelastic Timoshenko Beams with fractional derivative damping models [21], the application to multi-stepped Euler-Bernoulli beams under arbitrarily distributed loads carrying any number of concentrated elements [5],

the free vibration analysis of continuous bridges under vehicles as ambient excitation forces [22] and the application to cracked Timoshenko beams carrying spring-mass systems [23]. However, to the best knowledge of the authors, the NAT is only applied to multi-span and/or multi-stepped beams.

In the present paper, the NAT is extended to plane frame structures based on the Euler-Bernoulli beam theory with various combinative supports, hinges, and springs. Therefore, we systematically introduce a frame structure as a set of nodes, beams, bearings, springs, and external loads and formulate the corresponding boundary and interface conditions. Writing the system of equations in matrix form allows us to solve for the natural frequencies of the plane structure. This has to be done numerically. More than that, the general function to solve the governing equation for transversal vibrations is improved by using the novel approach introduced in [5]. This increases the accuracy of the results, especially when computing natural frequencies in high-frequency ranges. The proposed NAT is implemented in a MATLAB[®]-based code and its numerical performance is investigated at two exemplary frame structures.

2. Mechanical Models

2.1. Governing equations for a single beam

When considering vibrations in the two-dimensional space, the longitudinal and transversal deformation of an element are implicated. Let ℓ be the length of the considered beam with constant geometrical and material parameters along its local beam axis, where ρ is the density, E the Youngs Modulus, A the cross-section area, and I the area moment of inertia. With the position $\xi \in [0, \ell]$ and the time t , the differential equations for longitudinal vibrations are given by

$$\rho A \ddot{u}(\xi, t) = N'(\xi, t) + n(\xi, t), \quad (1a)$$

$$N(\xi, t) = EA u'(\xi, t). \quad (1b)$$

With $u(\xi, t)$ as the axial deformation, $N(\xi, t)$ defining the internal axial force and $n(\xi, t)$ the external axial loading force. Further, $()'$ denotes the derivative with

respect to ξ and $\dot{(\)}$ the derivative with respect to time. The differential equations for transversal vibrations governed by the Euler-Bernoulli beam theory read as

$$\rho A \ddot{w}(\xi, t) = V'(\xi, t) + q(\xi, t), \quad (2a)$$

$$V(\xi, t) = M'(\xi, t), \quad (2b)$$

$$M(\xi, t) = EI \psi'(\xi, t), \quad (2c)$$

$$w'(\xi, t) = -\psi(\xi, t). \quad (2d)$$

Where the transversal deflection $w(\xi, t)$ is described through the internal shear force $V(\xi, t)$, the internal bending moment $M(\xi, t)$, the rotation angle $\psi(\xi, t)$ and the external transversal loading force $q(\xi, t)$. When referring to the natural frequencies of a structure, the considered equation simplifies to a homogeneous differential equation, since it holds for the load forces $n = 0$ and $q = 0$. Assuming free harmonic vibrational behavior with the natural frequency ω the governing equations are

$$\frac{\partial^2 U(\xi)}{\partial \xi^2} + c^2 U(\xi) = 0, \quad (3)$$

$$\frac{\partial^4 W(\xi)}{\partial \xi^4} - \kappa^4 W(\xi) = 0, \quad (4)$$

with

$$c^2 = \frac{\rho}{E} \omega^2, \quad \kappa^4 = \frac{\rho A}{EI} \omega^2.$$

2.2. Frame structure

To introduce a frame structure formally, we extend the notation introduced in [24]. Let \mathcal{N} be the set of nodes, \mathcal{T} the set of beams, \mathcal{Q} the set of bearings, \mathcal{S} the set of springs and \mathcal{F} the set of external loads. For a frame structure $(\mathcal{N}, \mathcal{T}, \mathcal{Q}, \mathcal{S}, \mathcal{F})$ these sets have the following properties:

1. Each beam $m \in \mathcal{T}$ connects two nodes $k_0, k_\ell \in \mathcal{N}$ and holds constant parameters ρ_m, E_m, I_m, A_m . The beam m can either be connected rigidly or hinged at k_0 and k_ℓ .

2. Each node $k \in \mathcal{N}$ has a set of attached beams $\beta_k \subseteq \mathcal{T}$, a set of attached springs $\chi_k \subseteq \mathcal{S}$, external loads $\mathbf{F}_k^{ext} \in \mathcal{F}$ and external moments $M_k^{ext} \in \mathcal{F}$. Further, a bearing $\gamma_k \subseteq \mathcal{Q}$ can be attached at any node k .

Here, we assumed that the external forces and moments only act on the nodes. In general, also distributed loads acting on the beams are possible. However, due to the focus on the computation of natural frequencies, the influence of external loads is not further considered in Eq. (3) and Eq. (4). For a beam $m \in \mathcal{T}$ we define the tangent vector $\mathbf{t}_m = k_{\ell,m} - k_{0,m}$ and the normal vector $\mathbf{n}_m \perp \mathbf{t}_m$. The resulting internal force vector of beam $m \in \mathcal{T}$ is defined as

$$\mathbf{S}_m(\xi) = N_m(\xi) \cdot \mathbf{t}_m + V_m(\xi) \cdot \mathbf{n}_m. \quad (5)$$

2.3. Boundary and coupling conditions

With the definitions in Section 2.2 the boundary and interface conditions can now be formulated. First, the kinetics are defined by formulating the equilibrium of forces at each node k ,

$$\mathbf{F}_k = \sum_{m \in \beta_k} \mathbf{S}_{m|k} + \mathbf{Q}_k^L + \mathbf{F}_k^{ext} + \mathbf{F}_k^L = 0, \quad (6)$$

where, $\sum \mathbf{S}_{m|k}$ is the sum of each beam's internal forces, \mathbf{Q}_k^L the reaction forces from bearings, \mathbf{F}_k^{ext} the external loading forces and \mathbf{F}_k^L the constrained forces due to springs. The equilibrium of moments at each node k reads

$$M_k = \sum_{m \in \beta_k} M_{m|k} + Q_k^R + M_k^{ext} + M_k^R = 0, \quad (7)$$

where, $\sum M_{m|k}$ is the sum of each beam's internal bending moment, Q_k^R the constrained rotational moments from bearings, M_k^{ext} the external loading moments and M_k^R the rotational moments due to springs. The terms in Eq. (6) and Eq. (7) that include springs are defined through Hooke's law,

$$\mathbf{F}_k^L = c_L(\mathbf{U}_k \cdot \boldsymbol{\zeta}) \cdot \boldsymbol{\zeta} \quad (8)$$

and

$$M_k^R = c_\psi \cdot \psi_k, \quad (9)$$

where c_L and c_ψ define the spring constants of the longitudinal and the rotational spring, respectively and ζ is the direction vector along the axis of the longitudinal spring. Ultimately \mathbf{U}_k and ψ_k describe the displacement and the rotation of node k , respectively. Next we formulate the coupling conditions for a node $k \in \mathcal{N} : |\beta_k| > 1$. Therefore, let $m_f \in \beta_k$ be a beam that is fixed in the set of beams connected at k . The compatibility condition of the resulting deformation \mathbf{U} of the beam m evaluated at the node k reads

$$\mathbf{U}_{m_f|k} = \mathbf{U}_{m|k} \quad \forall m \in \beta_k \setminus m_f. \quad (10)$$

To differentiate between rigid and hinged connections the set of attached beams β_k at a node $k \in \mathcal{N} : |\beta_k| > 1$ is divided into two subsets, so that $\beta_k = \beta_k^r \cup \beta_k^h$. Thus, β_k^r includes the beams that are rigidly connected with one another and β_k^h the beams that are attached at k with an hinge. To formulate the kinematic relations concerning rotations, let $m_r \in \beta_k^r$ be a rigidly connected beam at node k that is fixed in the set of rigidly connected beams at this node. For all $m \in \beta_k^r \setminus m_r$ the kinematic conditions for the rotation ψ of the beam m evaluated at the node k are

$$\psi_{m_r|k} = \psi_{m|k} \quad \forall m \in \beta_k^r \setminus m_r. \quad (11)$$

Furthermore, let $m_h \in \beta_k^h$ be a beam that is connected with a hinge at the node k and fixed in the set of beams with a hinged connection at this node. The kinetic conditions are

$$M_{m|k} = 0 \quad \forall m \in \beta_k^h \setminus m_h. \quad (12)$$

It is noteworthy that through the equilibrium equation Eq. (7) the condition $M_{m_h|k} = 0$ holds true. The boundary conditions due to applied bearings are

defined in the local coordinate system for bearings $[\zeta, \eta]$ with the corresponding unit vectors $\mathbf{e}_\zeta \perp \mathbf{e}_\eta$, see Table A.5 and read for the pinned bearing

$$\mathbf{U}_{m|k} = 0 \quad m \in \beta_k, \quad (13)$$

the roller

$$\mathbf{U}_{m|k} \cdot \mathbf{e}_\eta = 0 \quad m \in \beta_k, \quad (14)$$

the clamped bearing

$$\mathbf{U}_{m|k} = 0 \quad m \in \beta_k, \quad (15a)$$

$$\psi_{m|k} = 0 \quad m \in \beta_k^r, \quad (15b)$$

and the parallel guide

$$\mathbf{U}_{m|k} \cdot \mathbf{e}_\eta = 0 \quad m \in \beta_k, \quad (16a)$$

$$\psi_{m|k} = 0 \quad m \in \beta_k^r, \quad (16b)$$

respectively.

3. Local Solutions of the governing equations

The local solution of the differential equation Eq. (3) in the frequency domain reads as

$$U_m(\xi) = C_{m,1} \cos(c_m \xi) + C_{m,2} \sin(c_m \xi). \quad (17)$$

For the transversal vibrations, in this work, we refer to the *alternative ansatz* which differs from the conventionally used solutions. Therefore, its derivation is stated. When implementing the ansatz $W_{(\xi)} = e^{\lambda \xi}$, the equation Eq. (4) can be expressed with its characteristic polynomial

$$\lambda^4 - \kappa^4 = 0. \quad (18)$$

The four roots of the eigenvalue problem Eq. (18) are $\lambda_1 = +\kappa$, $\lambda_2 = +i\kappa$, $\lambda_3 = -\kappa$, and $\lambda_4 = -i\kappa$. Thus, a general solution that corresponds the real and complex roots of Eq. (18) needs to be found. Many publications refer to the commonly used ansatz

$$W_m(\xi) = C_{m,3} \cos(\kappa\xi) + C_{m,4} \sin(\kappa\xi) + C_{m,5} \cosh(\kappa\xi) + C_{m,6} \sinh(\kappa\xi). \quad (19)$$

In this publication, a different ansatz function for the general solution of the differential equation for transversal vibration is presented. When rewriting the ansatz $W(\xi) = e^{\lambda\xi}$ with the obtained roots λ_{1-4} , $W(\xi)$ can be expressed as

$$W_m(\xi) = C_{m,1}e^{+\kappa\xi} + C_{m,2}e^{-i\kappa\xi} + C_{m,3}e^{+\kappa\xi} + C_{m,4}e^{-\kappa\xi}. \quad (20)$$

Since the condition

$$\cos(\xi) + \sin(\xi) = \left(\frac{1}{2} + \frac{i}{2}\right) e^{-i\xi} + \left(\frac{1}{2} - \frac{i}{2}\right) e^{i\xi} \quad (21)$$

holds, the first two terms in Eq. (20) can be simplified as trigonometrical functions, whereas the last two terms in Eq. (20) are kept as exponential functions so that the general solution is

$$W_m(\xi) = C_{m,1} \cos(\kappa\xi) + C_{m,2} \sin(\kappa\xi) + C_{m,3}e^{\kappa\xi} + C_{m,4}e^{-\kappa\xi}. \quad (22)$$

After dividing the third term in Eq. (22) by $e^{\kappa L}$, so that

$$e^{\kappa\xi} \cdot e^{-\kappa L} = e^{\kappa(\xi-L)}, \quad (23)$$

the final general solution is

$$W_m(\xi) = C_{m,1} \cos(\kappa\xi) + C_{m,2} \sin(\kappa\xi) + C_{m,3}e^{\kappa(\xi-L)} + C_{m,4}e^{-\kappa\xi}. \quad (24)$$

In the alternative ansatz Eq. (24), hyperbolic functions are avoided in the general solution. The reason for that is the asymptotic form of hyperbolic functions.

As the value of ξ or ω increases, the hyperbolic function terms get extremely high, and therefore, handling with those high numbers becomes rather cumbersome and the computational effort increases drastically. Contrarily, the amplitudes of the exponential terms in the general solution Eq. (24) stay within the fixed interval $\mathcal{V} \in [e^{-\kappa L}, 1]$, see Figure 1. Hence, determining the natural frequency using this ansatz is much simpler and faster.

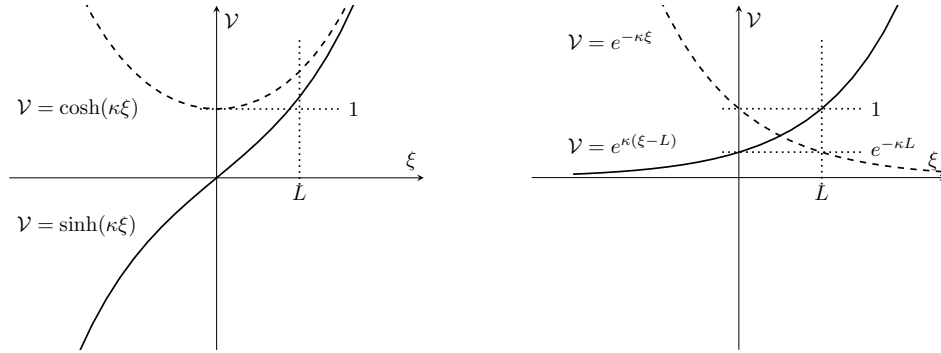


Figure 1: The difference of ansatz functions for the general solution. The hyperbolic- (left) and exponential approach (right).

To illustrate this, we investigate the condition number for the bending terms of the system matrix \mathbf{A} of a one-span beam, see Figure 2. The condition number gives information about the sensitivity of a linear system to small changes in a matrix. When using the Numerical Assembly Technique to determine the natural frequencies of a structure, a system matrix is generated. Depending on the number of beams, the size of this matrix can get rather big. Due to rounding errors, small changes in the system matrix could lead to instability of the linear system when choosing the common hyperbolic functions in the general solution. The proposed exponential and trigonometrical approach ensures stable computations even at high frequencies. The graphs in Figure 2 refer to the three different general solutions Eq. (19)→(a), Eq. (22)→(b) and Eq. (24)→(c).

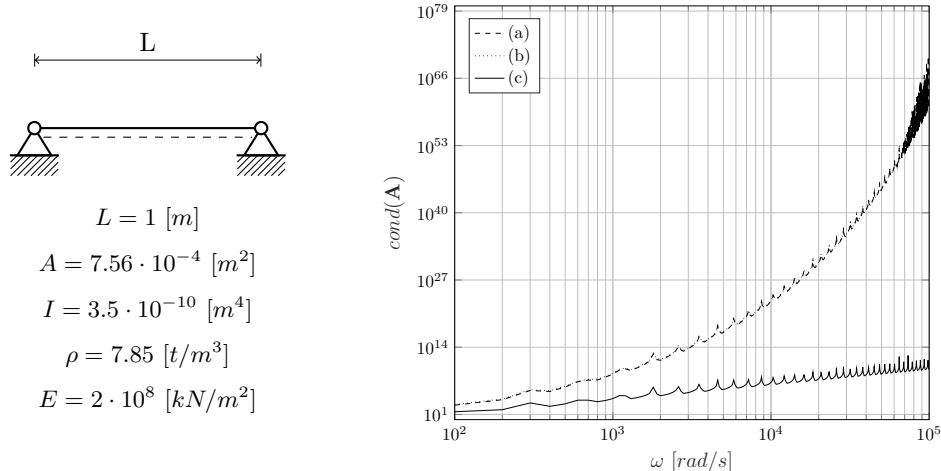


Figure 2: The condition number for a single span beam's system matrix.

It clearly shows in Figure 2 that the linear system based on the commonly used general solution (a), as well as the second approach (b), becomes quickly unstable for higher frequencies. The graphs of the solutions (a) and (b) coincide with this structure and rise exponentially in this double-logarithmic plot. But the instability of the linear system using the modified general solution (c) rises linearly in a relatively moderate manner. Thus, the evaluation of natural frequencies should therefore be improved by this change and has an effect when the natural frequencies need to be accurately determined, particularly for higher frequency ranges.

4. The Numerical Assembly Technique

In the Numerical Assembly Technique, the homogeneous solutions Eq. (19), Eq. (22) and Eq. (24) as well as Eq. (17), are used to fulfill the boundary and interface conditions, stated in Section 2, and therefore, the harmonic governing equations Eq. (3) and Eq. (4) are exactly satisfied. The system of equations is

$$\mathbf{A}(\omega)\mathbf{c} = \mathbf{0} \quad (25)$$

where \mathbf{c} is a $n \times 1$ vector $[\mathbf{c}_m, \mathbf{Q}]^T$ containing the integration constants \mathbf{c}_m and the bearing forces and moments \mathbf{Q} and \mathbf{A} forms the $n \times n$ asymmetric system matrix and only depends on ω . The size of the system of equations is defined as $n = |\mathcal{T}| \cdot 6 + |\mathcal{Q}|$. Each row of \mathbf{A} is obtained by inserting the homogeneous solutions into the boundary and interface conditions Eq. (6), Eq. (7), Eq. (10) to Eq. (14), Eq. (15a), Eq. (15b), Eq. (16a) and Eq. (16b), respectively. Non trivial solutions for ω fulfill the system of equations Eq. (25) when its determinant is zero,

$$f(\omega) = \det(\mathbf{A}) = 0. \quad (26)$$

Here, $f(\omega)$ is a continuous function with an infinite number of zero crossings and is often referred to as the eigen-, or frequency function. Each ω that fulfills the so-called characteristic equation Eq. (26) is an eigenvalue of the system of equations and, therefore, a natural frequency of the structure. In the present work, the zeros of $f(\omega)$ are determined using the Regular-Falsi method. This method gives accurate results over a rather short computation time and, meets therefore the expectations of this application. Implementing the calculated ω -values into our system of equations makes it possible to solve for the integration constants \mathbf{c}_m and the bearing forces and moments \mathbf{Q} representing the mode shapes to each natural frequency.

5. Numerical Results

5.1. Numerical Precision

When using the common trigonometric-hyperbolic ansatz Eq. (19) for arbitrary frame structures, one will sooner obtain inadequate results due to numerical inaccuracy when evaluating the frequency function $f(\omega)$. Especially, when the wanted natural frequency lies in a rather high-frequency range and/or the frequency function becomes lengthy e.g. for more complicated structures. Thus, numerical precision plays an important role. However, the computational performance can be improved by referring to the *alternative ansatz* Eq. (24). With this ansatz, the numerical results are more stable for higher frequencies

and rather complicated frequency functions and do not rely on a very high numerical precision. To illustrate this, in Figure 3, zoomed-in pictures show the frequency function $f(\omega)$ based on ansatz Eq. (19) of a frame structure in the area of the first four natural frequencies. Here, the frequency function is once evaluated with double precision and once using the variable precision arithmetic *vpa* in Matlab. We observe that for higher frequencies the frequency function becomes rather jagged for double precision. As a result, one can obtain multiple natural frequencies where there is only one expected.

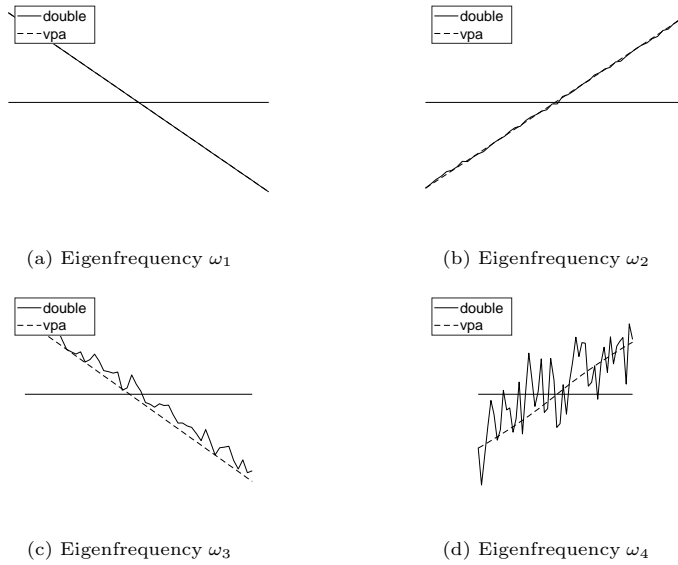


Figure 3: Zoomed-in pictures of the frequency function $f(\omega)$ at the eigenfrequencies ω_i . In all graphs $f(x_i)$ is plotted with $x_i \in [\omega_i - \epsilon; \omega_i + \epsilon]$, $\epsilon = 10^{-12}$.

5.2. Frame Structure

We present a test example of a structure consisting of two rigidly connected beams forming an arbitrary frame structure. The frame is pinned on one side and clamped on the other side, see Figure 4. The test example was modeled based on a steel profile, with the parameters $A_m = 7.56 \cdot 10^{-4} [m^2]$, $I_m = 3.5 \cdot 10^{-10} [m^4]$, $\rho_m = 7.85 [t/m^3]$ and $E_m = 2 \cdot 10^8 [kN/m^2]$ for each beam. The solution procedure was applied to this structure by using the three

ansatz functions (a)→Eq. (19), (b)→Eq. (22), (c)→Eq. (24) and the results were compared to a finite element computation with an alternating size of elements per beam, see Table 2. Also, the times to compute natural frequencies were compared between the NAT and the FEM approach, see Table 3. There, the computational time was taken for the last natural frequency computed using the FE Method that still lies within a range of a 10% deviation from the NAT result with ansatz (c) and compared to the computation time using the NAT with ansatz (c). Further, the condition number was plotted for this example and can be studied in Figure 6.

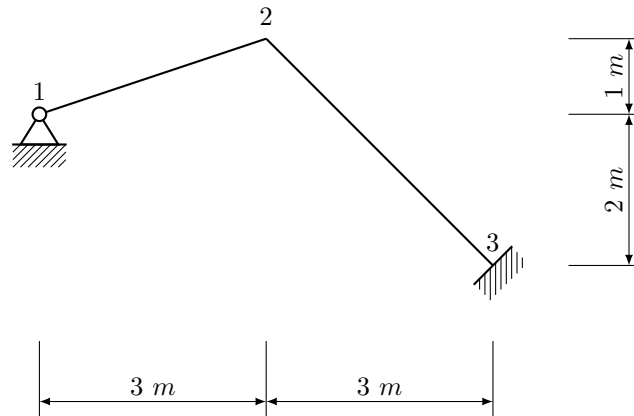


Figure 4: The modeled frame structure.

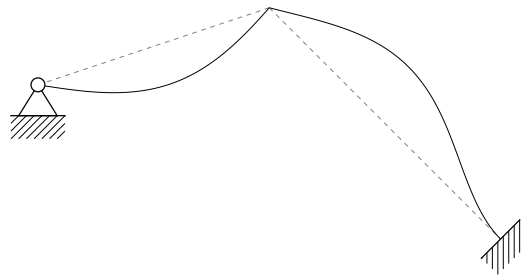


Figure 5: The first mode shape of the frame structure.

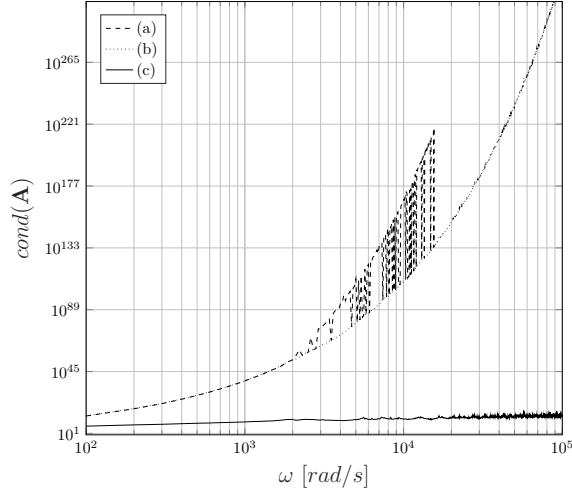


Figure 6: The condition number of the system matrix of the frame structure.

Table 1: The computation times of the frame structure.

Number of Frequency	FEM			NAT
	max. ω [rad/s] ¹	Elements per beam	t[s]	t[s]
2	4.8627	2	< 0.1	< 0.1
6	33.0061	4	< 0.1	< 0.1
13	128.3669	8	< 0.1	< 0.1
32	716.3521	16	< 0.1	< 0.1
73	3510.2522	32	< 0.1	0.12569
151	14234.4738	64	0.1068	0.43859
320	59048.7810	128	0.9619	0.51866
702	243982.2853	256	15.7096	2.2451
1594	957605.9388	512	192.2587	42.2335
3195	2771277.8678	1024	1595.0565	42.2877

¹last frequency computed with FEM that has less than 10% deviation from NAT computation with Ansatz (c)

Table 2: The natural frequencies of the frame structure in [rad/s].

Number of Natural Frequency	NAT						FEM		
	double			vpa			Elements per Beam		
	(a)	(b)	(c)	(a)	(b)	(c)	16	32	64
1	3.1094	3.1094	3.1094	3.1094	3.1094	3.1094	3.1094	3.1094	3.1094
2	4.8078	4.8078	4.8078	4.8078	4.8078	4.8078	4.8078	4.8078	4.8078
3	10.4144	10.4144	10.4144	10.4144	10.4144	10.4144	10.4144	10.4144	10.4144

15	162.8158	162.8160	162.8160	162.8160	162.8160	162.8160	163.7454	162.8787	162.8200
16	174.6030	174.6036	174.6036	174.6036	174.6036	174.6036	175.3495	174.6525	174.6067
17	201.9954	202.0324	202.0324	202.0324	202.0324	202.0324	203.9897	202.1665	202.0409

31		634.9490	634.9490	634.9490	634.9490	634.9490	688.0855	638.8745	635.2119
32		675.0622	675.0622	675.0622	675.0622	675.0622	716.3521	677.3190	675.2117
33		708.8620	708.8620	708.8620	708.8620	708.8620	787.7197	714.2016	709.2205
	
48		1498.5735	1498.5735	1498.3202	1498.5735	1498.5735	1848.5917	1523.7303	1500.7542
49		1526.1712	1526.1712	1527.1223	1526.1712	1526.1712	1923.3839	1565.8748	1528.9541
50		1618.8520	1618.8520	1581.1209	1618.8520	1618.8520	2003.3543	1663.6016	1622.9055
	
72		3099.1823	3099.1823		3099.1823	3099.1823	21006.9000	3386.8400	3120.1627
73		3219.5726	3219.5726		3219.5726	3219.5726	22796.4503	3510.2522	3248.4805
74		3289.0796	3289.0796		3289.0796	3289.0796	25373.8867	3711.2534	3306.7830
	
150		5146.4523	5146.4523		5146.4523	5146.4523		53266.5249	13871.6132
151		5198.0249	5198.0249		5198.0249	5198.0249		54623.1788	14234.4738
152		5357.7191	5357.7191		5357.7191	5357.7191		57991.3441	14646.4119
	
188		20082.8678	20082.8678		20082.8678	20082.8678		171783.6588	23671.7495
189		20161.3979	20161.3979		20161.3979	20161.3979		174609.8040	23903.3555
190		20449.5667	20449.5667		20449.5667	20449.5667		176350.0940	24275.7074
	
191		20516.9051	20516.9051		20516.9051	20516.9051			24345.0237
192		20733.0092	20733.0092		20733.0092	20733.0092			24662.7192
193		20919.7970	20919.7970		20919.7970	20919.7970			25015.2626
	
219			26794.1655		26794.1655	26794.1655			33423.5651
220			26915.9936		26915.9936	26915.9936			33780.5983
221			27220.7782		27220.7782	27220.7782			34152.4567
		
380			74088.3050		74088.3050	74088.3050			351135.7772
381			74411.2521		74411.2521	74411.2521			352652.5927
382			74862.5654		74862.5654	74862.5654			353569.1257
		
1735			997062.8183		997062.8183	997062.8183			..
1736			998652.9269		998652.9269	998652.9269			..
1737			999016.8478		999016.8478	999016.8478			..
		

In Figure 6 it can be observed that the condition number for the system matrix of the frame structure using ansatz (c) stays low even for high frequencies which is an indicator for a stable system of equations. Whereas the condition

number for the system matrices using ansatz (a) and (b) increases drastically with rising frequency ω . The commonly used ansatz (a) even forms additional peaks before reaching complete failure. Table 2 shows that the natural frequencies computed with the NAT are more accurate than the FEM results. Numbers are underlined if they differ from the NAT solution using ansatz (c). A result is colored gray when it passed the 10% deviation from the NAT solution using ansatz (c). When there is a blank cell in the table, no result was able to be computed, i.e. the computation failed. It is also noticeable that regarding the NAT, the ansatz (c), the presented *alternative ansatz*, performs better than the other two general solutions. While even using a 'lower' double-precision, the NAT with ansatz (c) outperforms the FEM as well as the other two ansatz functions. As noticed, the two dots in the last row of the columns for ansatz (c) indicate that the limit has not yet been reached there, so even higher natural frequencies can be computed using this ansatz. In Table 3 the computational times for the FEM look promising for lower natural frequencies but rise tremendously as the frequency range increases. Contrarily, the times to compute the same natural frequencies using the NAT with ansatz (c) increase rather moderately and stay low for immensely high frequencies.

5.3. Bridge

A reinforced concrete bridge was modeled regarding the parameters $L = 20[m]$, $E = 31 \cdot 10^6[kN/m^2]$, $\rho = 2.3[t/m^3]$ for all beams. The beams 1 - 3 share the parameters $A = 12[m^2]$, $I = 40[m^4]$ and for the remaining beams 4 - 5 the parameters are $A = 9[m^2]$, $I = 30[m^4]$.

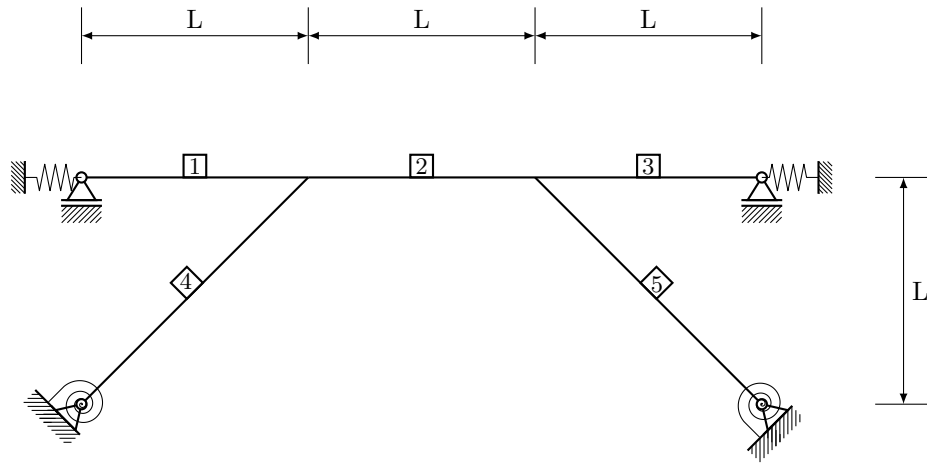


Figure 7: The modeled bridge.

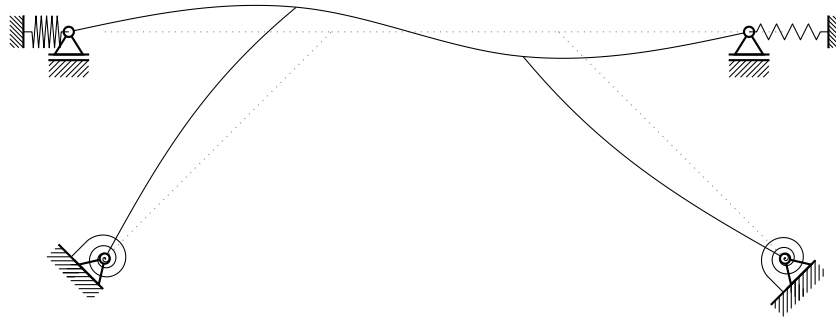


Figure 8: The first mode shape of the bridge.

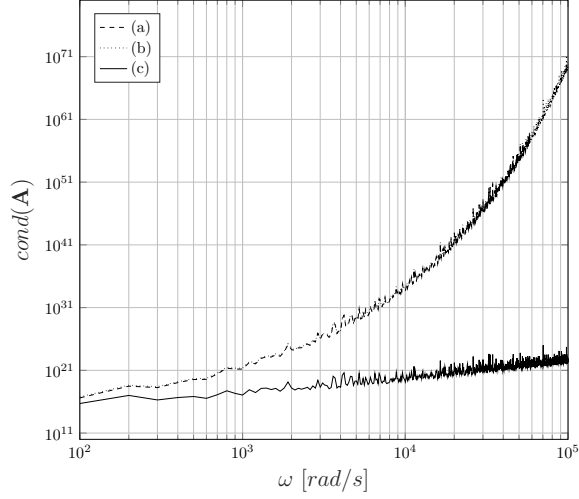


Figure 9: The condition number of the system matrix of the bridge.

Table 3: The computation times of the bridge.

Number of Frequency	FEM			NAT
	max. ω [rad/s] ²	Elements per beam	t[s]	t[s]
11	418.2554	2	< 0.1	< 0.1
25	1223.6150	4	< 0.1	< 0.1
44	2547.1030	8	< 0.1	0.25898
74	4837.9021	16	< 0.1	1.0005
130	9685.2435	32	< 0.1	1.0574
223	18003.4972	64	< 0.1	4.5552
433	38425.0172	128	1.0901	4.7907
805	75794.2360	256	12.9402	22.3849
1586	157012.4639	512	104.0063	24.0491
3194	330080.3245	1024	815.8332	25.2141

²last frequency computed with FEM that has less than 10% deviation from NAT computation with Ansatz (c)

Table 4: The natural frequencies of the bridge in [rad/s].

Number of Natural Frequency	NAT						FEM		
	double			vpa			Elements per Beam		
	(a)	(b)	(c)	(a)	(b)	(c)	16	32	64
1	37.9854	37.9854	37.9854	37.9854	37.9854	37.9854	37.9856	37.9855	37.9854
2	74.2871	74.2871	74.2871	74.2871	74.2871	74.2871	74.2875	74.2872	74.2871
3	105.7450	105.7450	105.7450	105.7450	105.7450	105.7450	105.7487	105.7459	105.7453

73	4461.7242	4461.7242	4461.7242	4461.7242	4461.7242	4461.7242	4753.2843	4539.9982	4480.5927
74	4473.8551	4473.8551	4473.8551	4473.8551	4473.8551	4473.8551	4837.9021	4634.3395	4515.8803
75	4515.0470	4515.0470	4515.0470	4515.0470	4515.0470	4515.0470	5000.6678	4657.4950	4559.9003

129	8812.4941	8812.4941	8812.4941	8812.4941	8812.4941	8812.4941	12994.3482	9646.0261	8965.7722
130	8853.3989	8853.3989	8853.3989	8853.3989	8853.3989	8853.3989	13693.3704	9685.2435	9000.0630
131	8862.1473	8862.1475	8862.1475	8862.1475	8862.1475	8862.1475	14437.5183	9878.7665	9071.5678

222		16416.1027	16416.1027	16416.1027	16416.1027	16416.1027	156994.8526	20342.0473	17874.0744
223		16527.6906	16527.6906	16527.6906	16527.6906	16527.6906	165670.7114	21219.2334	18003.4972
224		16545.6271	16545.6271	16545.6271	16545.6271	16545.6271	169638.2781	21975.3448	18225.9889

235		17514.5070	17514.5070	17514.5070	17514.5070	17514.5070	212717.0285	29380.2136	19376.7279
236		17545.6329	17545.6329	17545.6329	17545.6329	17545.6329	214599.6433	30468.3455	19426.6437
237		17629.9634	17629.9634	17629.9634	17629.9634	17629.9634	214602.7984	30985.1054	19537.4222

475		38742.1566	38742.1566	38742.1566	38742.1566	38742.1566		858548.1299	122440.6046
476		38762.7334	38762.7334	38762.7334	38762.7334	38762.7334		860629.4273	122704.7380
477		38890.8164	38890.8164	38890.8164	38890.8164	38890.8164		860630.2312	123645.1451

502		41198.3553	41198.3553	41198.3553	41198.3553	41198.3553			166664.8265
503		41202.1461	41202.1461	41202.1461	41202.1461	41202.1461			170118.4611
504		41283.0173	41283.0173	41283.0173	41283.0173	41283.0173			172312.0002

761			64851.1221	64851.1221	64851.1221	64851.1221			1153652.4623
762			64912.1209	64912.1210	64912.1209	64912.1209			1162563.6568
763			64983.7916	64983.7918	64983.7916	64983.7916			1170839.8358

955			82573.2725		82573.2725	82573.2725			3442594.0097
956			82613.2799		82613.2799	82613.2799			3444776.2656
957			82772.9680		82772.9680	82772.9680			3444776.4683

1014			88010.7113			88010.7113			
1015			88090.9183			88090.9183			
1016			88095.6490			88095.6490			

The results of the bridge behave, as expected, similar to the results of the frame structure and matching tendencies can be observed among the three different ansatz functions and the FEM results. In both cases, the NAT using the *alternative ansatz* delivers outstanding results and outperforms the conventional ansatz functions and the FEM computations in many ways.

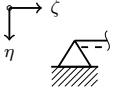



6. Conclusion

In the present paper, we extended the NAT to the computation of natural frequencies of plane frame structures based on the Euler-Bernoulli beam theory. Since analytic solutions are used, no discretization refinement is necessary and exact results are obtained. We have formally introduced a frame structure as a set of nodes, beams, bearings, springs, and external loads. This allows us to formulate the boundary and interface conditions in a systematic way for an arbitrary system. In combination with the *alternative ansatz*, the implemented method provides stable computations of natural frequencies also for higher frequency ranges and complicated structures with multiple beams.

In future work, various extensions of the presented method should be easily possible. This includes the consideration of concentrated masses, dampers, and cracked beams in the two-dimensional setting. Furthermore, the extension to space frames and non-linear beam geometries would be an interesting research direction. Implementing the Timoshenko beam theory in the existing code can also be considered.

Appendix A. Appendix

Table A.5: A list of the different support types and its support conditions.

name of support type	symbolic representation	supporting conditions
Pinned		$M = 0$ $U_{\zeta} = 0$ $U_{\eta} = 0$
Roller		$M = 0$ $S_{\zeta} = 0$ $U_{\eta} = 0$
Clamped		$\psi = 0$ $U_{\zeta} = 0$ $U_{\eta} = 0$
Parallel guide		$\psi = 0$ $S_{\zeta} = 0$ $U_{\eta} = 0$

References

- [1] D. Dinkler, Einführung in die Strukturdynamik [An introduction to structural dynamics], Springer Vieweg, Wiesbaden, Germany, 2016. doi:<https://doi.org/10.1007/978-3-658-19815-2>.
- [2] S. S. Rao, Vibration of continuous systems, John Wiley & Sons, Hoboken, New Jersey, USA, 2019. doi:<https://doi.org/10.1002/9781119424284>.
- [3] R. Gasch, K. Knothe, Strukturdynamik: Bd. 2. Kontinua Und Ihre Diskretisierung [Structural dynamics: Vol. 2. Continua and discretization], Springer Verlag, Berlin, Germany, 1989.
- [4] W. Schiehlen, P. Eberhard, Technische Dynamik [Technical dynamics], Springer Vieweg, Wiesbaden, Germany, 2017. doi:<https://doi.org/10.1007/978-3-658-31373-9>.
- [5] M. Klanner, K. Ellermann, Steady-state linear harmonic vibrations of multiple-stepped Euler-Bernoulli beams under arbitrarily distributed loads carrying any number of concentrated elements, J. Appl. Comput. Mech. 14 (1) (2020) 31–50. doi:<https://doi.org/10.24132/acm.2020.583>.
- [6] P. Mario, H. K. Young, Structural dynamics: Theory and computation, Spinger Nature, Cham, Switzerland, 2019. doi:<https://doi.org/10.1007/978-3-319-94743-3>.
- [7] J. Banerjee, A. Ananthapuvirajah, Free vibration of functionally graded beams and frameworks using the dynamic stiffness method, J. Sound Vib. 422 (2018) 34–47. doi:<https://doi.org/10.1016/j.jsv.2018.02.010>.
- [8] S. Caddemi, I. Calio, Exact closed-form solution for the vibration modes of the Euler-Bernoulli beam with multiple open cracks, J. Sound Vib. 327 (3-5) (2009) 473–489. doi:<https://doi.org/10.1016/j.jsv.2009.07.008>.
- [9] J. Banerjee, Free vibration of beams carrying spring-mass systems- A dynamic stiffness approach, Comput. Struct. 104 (2012) 21–26. doi:<https://doi.org/10.1016/j.compstruc.2012.02.020>.

- [10] J. Banerjee, Free vibration of axially loaded composite Timoshenko beams using the dynamic stiffness matrix method, *Comput. Struct.* 69 (2) (1998) 197–208. doi:[https://doi.org/10.1016/S0045-7949\(98\)00114-X](https://doi.org/10.1016/S0045-7949(98)00114-X).
- [11] C. N. Bapat, C. Bapat, Natural frequencies of a beam with non-classical boundary conditions and concentrated masses, *J. Sound Vib.* 112 (1) (1987) 177–182.
- [12] T. A. El-Sayed, S. H. Farghaly, A normalized transfer matrix method for the free vibration of stepped beams: comparison with experimental and FE (3d) methods, *Shock Vib.* 2017 (2017). doi:<https://doi.org/10.1155/2017/8186976>.
- [13] M. Attar, A transfer matrix method for free vibration analysis and crack identification of stepped beams with multiple edge cracks and different boundary conditions, *Int. J. Mech. Sci.* 57 (1) (2012) 19–33. doi:<https://doi.org/10.1016/j.ijmecsci.2012.01.010>.
- [14] G. Š. Rončević, B. Rončević, A. Skoblar, R. Žigulić, Closed form solutions for frequency equation and mode shapes of elastically supported Euler-Bernoulli beams, *J. Sound Vib.* 457 (2019) 118–138. doi:<https://doi.org/10.1016/j.jsv.2019.04.036>.
- [15] A. Ghannadiasl, S. K. Ajirlou, Analytical solution of dynamic analysis of cracked Euler-Bernoulli beam with elastic boundary condition by GFM, *Rom. J. Acoust. Vib.* 15 (2) (2018) 100–107.
- [16] H. Han, D. Cao, L. Liu, A new approach for steady-state dynamic response of axially functionally graded and non-uniformed beams, *Compos. Struct.* 226 (2019) 111270. doi:<https://doi.org/10.1016/j.compstruct.2019.111270>.
- [17] A. Burlon, G. Failla, F. Arena, Exact stochastic analysis of coupled bending-torsion beams with in-span sup-

- ports and masses, *Probabilistic Eng. Mech.* 54 (2018) 53–64.
doi:<https://doi.org/10.1016/j.probengmech.2017.07.002>.
- [18] S. Di Lorenzo, C. Adam, A. Burlon, G. Failla, A. Pirrotta, Flexural vibrations of discontinuous layered elastically bonded beams, *Compos. B. Eng.* 135 (2018) 175–188.
doi:<https://doi.org/10.1016/j.compositesb.2017.09.059>.
- [19] G. Failla, An exact modal analysis approach to vibration analysis of structures with mass-spring subsystems and rotational joints, *J. Sound Vib.* 438 (2019) 191–219. doi:<https://doi.org/10.1016/j.jsv.2018.09.025>.
- [20] G. Failla, M. Di Paola, A. Pirrotta, A. Burlon, I. Dunn, Random vibration mitigation of beams via tuned mass dampers with spring inertia effects, *Meccanica* 54 (9) (2019) 1365–1383.
doi:<https://doi.org/10.1007/s11012-019-00983-8>.
- [21] M. Klanner, M. S. Prem, K. Ellermann, Steady-state harmonic vibrations of viscoelastic Timoshenko beams with fractional derivative damping models, *J. Appl. Mech.* 2 (4) (2021) 797–819.
doi:<https://doi.org/10.3390/applmech2040046>.
- [22] G. Tan, W. Wang, Y. Jiao, Z. Wei, Free vibration analysis of continuous bridge under the vehicles, *Struct. Eng. Mech.* 61 (3) (2017) 335–345.
doi:<https://doi.org/10.12989/sem.2017.61.3.335>.
- [23] G. Tan, J. Shan, C. Wu, W. Wang, Free vibration analysis of cracked Timoshenko beams carrying spring-mass systems, *Struct. Eng. Mech.* 63 (4) (2017) 551–565. doi:<https://doi.org/10.12989/sem.2017.63.4.551>.
- [24] D. Pölz, M. H. Gfrerer, M. Schanz, Wave propagation in elastic trusses: An approach via retarded potentials, *Wave Motion* 87 (2019) 37–57.
doi:<https://doi.org/10.1016/j.wavemoti.2018.06.002>.